Mechanisms of Creep Deformation in Mg-Sc–Based Alloys

B.L. MORDIKE, I. STULÍKOVÁ, and B. SMOLA

Binary Mg-Sc alloys show only a very weak age-hardening response due to the low diffusivity of Sc in Mg and exhibit inferior creep resistance compared to WE alloys. The addition of a small amount of Mn (<1.5 wt pct) improves their creep behavior markedly, decreasing the minimum creep rates by up to about two orders of magnitude at temperatures above 300 °C compared to WE alloys. This is due to the precipitation of fine Mn_2Sc phase basal discs, which are very effective obstacles in controlling creep at temperatures at which cross-slip of basal dislocations and nonbasal slip are the rate controlling mechanisms. The addition of Ce improves the creep resistance even more due to the effect of the grain boundary eutectic. The effect of Mn_2Sc discs can still be seen in alloys with a low Sc content (~1 wt pct) and with the addition of rare earth (RE) elements (Gd, Y, Ce ~4 wt pct). Very thin hexagonal plates containing RE and Mn, which lie parallel to the basal plane of the Mg matrix, augment the effect of the Mn_2Sc precipitates at elevated temperatures (~250 °C). The triangular arrangement of prismatic plates of metastable or stable phases of Mg-RE systems controls effectively the motion of basal dislocations during the creep of these alloys at elevated or high temperatures. The combined control of basal slip, cross-slip of basal dislocations, and of nonbasal slip in low Sc content alloys ensures minimum creep rates of about one order of magnitude lower than those observed in WE alloys, both at elevated and high temperatures.

I. INTRODUCTION

MAGNESIUM–rare earth (RE) alloys, such as WE43 and WE54, are recognized and used as high-performance lightweight constructional materials for sustained applications up to 250 °C. Nevertheless, they do not achieve the outstanding creep resistance of the thorium containing Mg alloys (ZH62, HZ32), which can operate at temperatures up to 350 °C.[1,2] Since thorium-containing Mg alloys are being phased out due to the slight radioactivity of Th, it was apparent that the only possibility to improve the high-temperature creep resistance beyond that of WE alloys was to turn to another Mg-RE system. The Mg-Sc system was promising for several reasons:

(a) alloying with Sc increases the melting point of the Mg-Sc solid solution (it is the only peritectic system among the Mg-RE alloys);[3]
(b) the high melting point of Sc compared to other REs (1541 °C) signifies a lower diffusivity in Mg;
(c) the density of Sc (2989 kg/m^3) is significantly lower than other REs; and
(d) alloying with other elements that form intermetallic compounds with Sc or complex precipitates with Sc and Mg might improve further the high-temperature properties.

The development of highly creep-resistant magnesium alloys based on alloying with scandium encompassed an investigation of squeeze-cast binary Mg-Sc, ternary Mg-Sc-Mn, quaternary Mg-Sc-Ce-Mn, Mg-Y-Sc-Mn, Mg-Gd-Sc-Mn, Mg-Ce-Sc-Mn, and complex Mg-Y-Nd-Sc-Mn alloys. The results of the creep behavior of the alloys in the temperature range of 200 °C to 350 °C and correlated with the corresponding structure are summarized and discussed here.

II. EXPERIMENTAL DETAILS

Almost all alloys investigated were squeeze cast at ZfW gGmbH (Clausthal, Germany). The starting materials were metallic Sc, Gd, Ce, and Y stirred into molten Mg or Mg-Mn (1.56 wt pct) master alloy (binary or ternary and quaternary alloys). Residual quantities of the MgSc15Mn1 alloy and Mg-Nd (12.0 wt pct, minimum, 11.5 wt pct Nd-MEL) master alloy were used for cast Mg-Y-Nd-Sc-Mn. Squeeze casting was carried out at an applied pressure of about 130 MPa in a protective atmosphere (Ar-SF_6). Only MgSc15 and MgSc19 were sand cast and ingot cast, respectively, by MEL (Magnesium Elektron Ltd., Manchester, United Kingdom). Table I summarizes the composition of the cast alloys as determined by atomic absorption.

Tensile creep tests were carried out in the temperature range 200 °C to 350 °C at stresses from 30 to 80 MPa to determine the minimum creep strain rates. Tests were also carried out at 40 MPa with increments in the temperature of 25 °C from 200 °C to 350 °C. The time dependence of the creep strain rate was continuously evaluated, and if the rate remained constant for a sufficient period, within experimental error, the load was reduced to zero in preparation for the next temperature. The creep strain rate measured was taken as the minimum creep rate corresponding to the load and temperature. The temperature was increased in the unloaded condition after which the specimen was reloaded.

In addition, tests were performed at a constant temperature of 300 °C and the stress was increased in steps of 10 MPa over the range from 30 to 80 MPa. The minimum creep strain rates determined from the standard tests (at the same

B.L. MORDIKE, Professor Emeritus, is with the Institute of Materials Engineering and Technology, TU Clausthal, 38678 Clausthal, Germany. I. STULÍKOVÁ and B. SMOLA, Associate Professors, are with the Faculty of Mathematics and Physics, Charles University, 121 16 Prague, Czech Republic, and all authors are with Zentrum für Funletions werestoffe, 38678 Clausthal-Zellerfeld, Germany. Contact e-mail: smola@met.mff.cuni.cz

This article is based on a presentation made in the symposium entitled "Phase Transformations and Deformation in Magnesium Alloys," which occurred during the Spring TMS meeting, March 14–17, 2004, in Charlotte, NC, under the auspices of ASM-MSCTS Phase Transformations Committee.

Table I. Composition (Weight Percent) and Thermal Treatment of Alloys

Alloy	Sc	Mn	Ce	Gd	Y	Nd	T4 (°C/h)	T5 or T6 (°C/h)
MgSc10	10.14	—	—	—	—	—	600/16	T4 + 230/24
MgSc11	11.11	—	—	—	—	—	600/16	T4 + 230/24
MgSc15	14.54	—	—	—	—	—	600/16	T4 + 230/24
MgSc19	19.09	—	—	—	—	—	600/16	T4 + 230/24
MgSc6Mn1	5.9	1.6	—	—	—	—	—	275/60
MgSc15Mn1	15.2	1.4	—	—	—	—	—	275/60
MgSc6Ce4Mn1	6.3	1.5	4.2	—	——	—	—	275/60
MgSc9Ce3Mn1	9.0	1.5	3.2	—	—	—	—	250/192
MgGd5Sc1Mn1	0.26	1.53	—	4.64	—	—	—	200/96
MgGd5Sc1Mn1	0.34	1.49	—	5.08	—	—	—	200/96
MgGd10Sc1Mn1	0.91	1.3	—	9.63	—	—	—	200/72
MgY4Sc1Mn1	0.73	1.11	—	—	3.88	—	—	275/48
MgY4Sc1Mn1	0.77	1.3	—	—	4.52	—	—	275/48
MgCe3Sc1Mn1	0.92	1.13	2.84	—	—	—	—	275/42
MgY4Nd2Sc1Mn1	1.28	1.18	—	—	3.71	2.12	—	200/45

conditions—stress and temperature) and change tests are comparable.

Isochronal annealing (step by step 30 °C/30 min) was carried out in the temperature range 20 °C to 600 °C to find the regions of the phase transformations. The conditions for peak age hardening (T6 or T5) were found by an isothermal heat treatment. Isochronal annealing involved continuous heating in an oil bath up to 240 °C or in furnace with Ar protective atmosphere for higher temperatures. Each treatment involved removing the specimen and quenching in liquid nitrogen or water. Isothermal annealing was carried out on specimens wrapped in protective steel foil and followed by quenching in water.

The phase transformations were monitored by the measurement of the relative electrical resistivity changes measured at 77 K and by Vickers hardness measurements (HV3) at room temperature. Relative electrical resistivity changes were obtained to within an accuracy of 10^{-4} by means of the direct current four-point method with a dummy specimen in series. The effect of a parasitic thermoelectromotive force was eliminated by a change in polarity. A decrease in the relative resistivity changes during isochronal annealing is usually caused by an increase in the purity of the majority phase due to precipitation. Dissolution of precipitated phases leads to an increase in the relative resistivity changes.

The precipitation microstructure of alloys in selected states of isochronal treatment, after a T5 aging treatment and after creep at 350 °C (30 or 40 MPa), was determined by transmission electron microscopy (TEM). The phases present were analyzed using electron diffraction and energy-dispersive X-ray microanalysis.

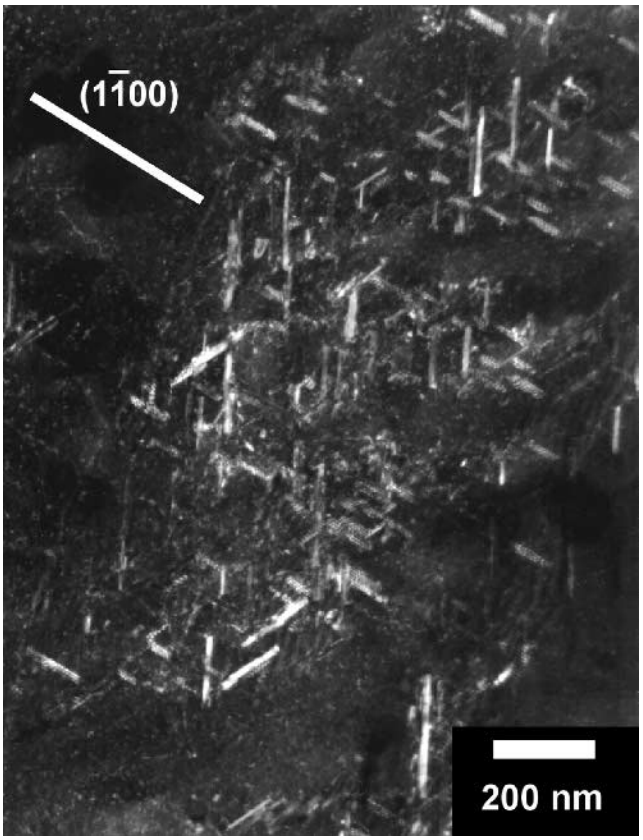

Fig. 1—Needlelike precipitates parallel to all equivalent $<11\bar{2}0>_{Mg}$ directions of α-Mg matrix in MgSc11 after isochronal annealing up to 330 °C. Dark field in precipitate reflection, near $[11\bar{2}3]_{Mg}$ pole.

III. RESULTS

A. *Binary Mg-Sc Alloys*

The Sc segregation, observed in the as-cast condition, disappeared after a solutionizing treatment, but large complex particles containing Sc still remained. The changes in the relative resistivity, in response to isochronal annealing, were very small.[4] This indicates that only a very low volume fraction of precipitates developed during annealing; in fact, only a few nests of needlelike precipitates in $<11\bar{2}0>$ directions were observed *via* TEM in MgSc11 after annealing up to 330 °C (Figure 1). Hardly any hardening on isothermal annealing was observed (Figure 2). All Mg-Sc alloys had significantly higher creep rates than the commercial alloy WE43 (Figure 3).[5,6] The difference decreases with increasing Sc content, but WE43 always showed the lowest minimum creep rate regardless of the initial treatment T4, as cast or T6. The minimum creep rate $\dot{\varepsilon}_s$ is usually expressed as

$$\dot{\varepsilon}_s = A \cdot \sigma^n \cdot \exp(Q_C/kT)$$

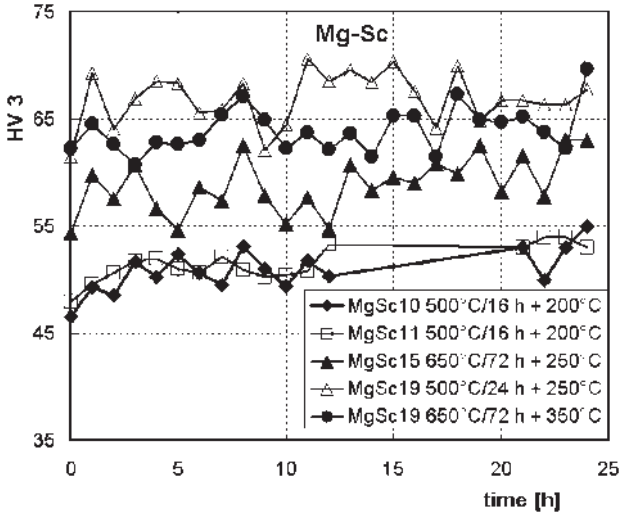

Fig. 2—Hardness response of selected binary Mg-Sc alloys to the isothermal annealing.

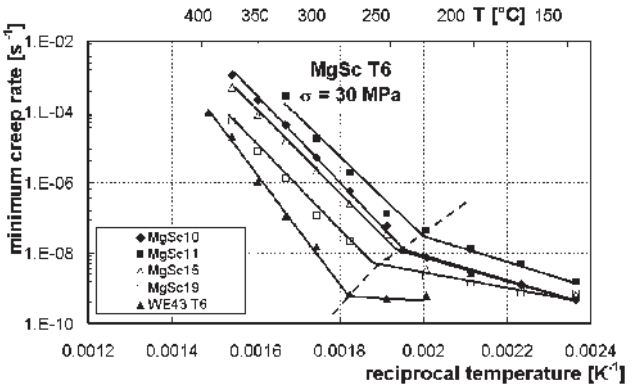

Fig. 3—Temperature dependence of minimum creep rate for binary Mg-Sc alloys compared to WE43.

where A is a constant, σ the applied stress, Q_C the activation energy for creep, and k the Boltzmann constant. Two temperature ranges with different values of Q_C were found for Mg-Sc alloys as with other RE-containing Mg alloys.[7,8] The transition temperature shifts to higher temperatures with increasing Sc content. The stress exponents n for T4- and T6-treated alloys in the high-temperature range (300 °C) were found to be 4.5 to 6.5 independent of the Sc content[9] (Table II).

B. *Mg-Sc-(Ce)-Mn Alloys with High Sc Content*

The choice of manganese as an addition to Mg-Sc alloys was supported by calculations of thermodynamic equilibrium based on the Mg-Sc-Mn ternary phase diagram. Only a T5 heat treatment is possible in the MgScMn and MgScCeMn alloys studied.[10,11] The precipitation process is characterized by the development of phases observed in the Sc-Mn and Mg-Ce systems. A very dense dispersion of fine Mn_2Sc spherical particles (diameter ~6 nm) developed during the T5 temper of MgSc15Mn1 alloy (Figure 4). Mn_2Sc particles have the form of discs (diameter ~20 nm, thickness ~5 nm, dense dispersion) parallel to the basal planes in the

Table II. Stress Exponents n for Various Alloys at 300 °C in Denoted Stress Range

Alloy	Temper	Stress Range (MPa)	Stress Exponent
MgSc10	T4	20 to 45	6.5
	T6	30 to 60	4.5
MgSc11	T6	20 to 40	6.5
MgSc15	T4	20 to 40	5
	T6	20 to 40	6.5
MgSc19	T4	20 to 45	6.5
	T6	20 to 40	6.5
MgSc6Mn1	as cast	20 to 40	5
	T5	20 to 40	5
MgSc6Mn1	as cast	40 to 60	9.5
	T5	40 to 60	10
MgSc15Mn1	as cast	20 to 40	5
	T5	20 to 40	5
MgSc15Mn1	as cast	40 to 60	9
	T5	40 to 70	10
MgSc6Ce4Mn1	as cast	20 to 40	3
	T5	20 to 40	3
MgSc6Ce4Mn1	as cast	40 to 70	10
	T5	40 to 60	10
MgSc9Ce3Mn1	as cast	20 to 40	3
	T5	20 to 40	3
MgSc9Ce3Mn1	as cast	40 to 70	10
	T5	40 to 70	10
MgGd10Sc1Mn1	as cast	30 to 50	7.5
MgGd5Sc1Mn1	as cast	30 to 50	7.5
MgY4Sc1Mn1	as cast	30 to 50	8
MgCe3Sc1Mn1	as cast	30 to 50	6

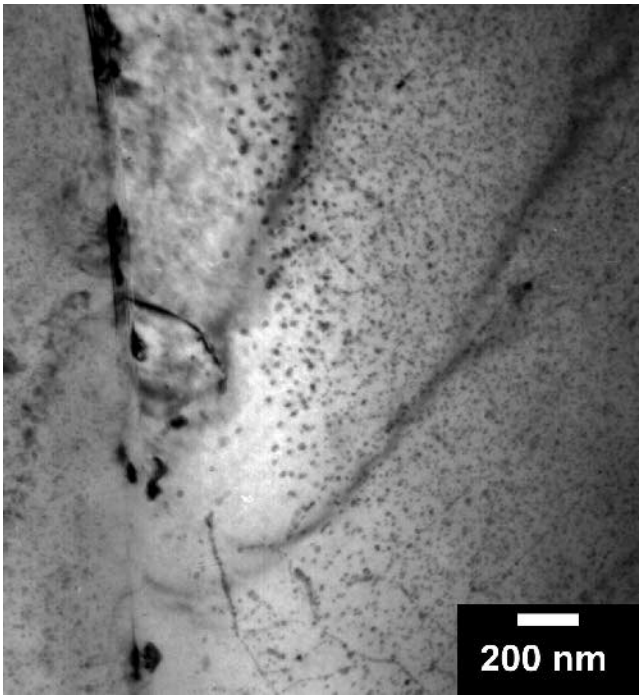

Fig. 4—Fine spherical particles of Mn_2Sc phase in T5-treated MgSc15Mn1 alloy. Bright field-structure contrast.

T5-treated MgSc6Ce4Mn1 alloy. Moreover, coarser $Mg_{12}Ce$ rectangular particles (~100 × 250 nm), elongated in the [0001] direction, precipitated within the grains (Figure 5).[12]

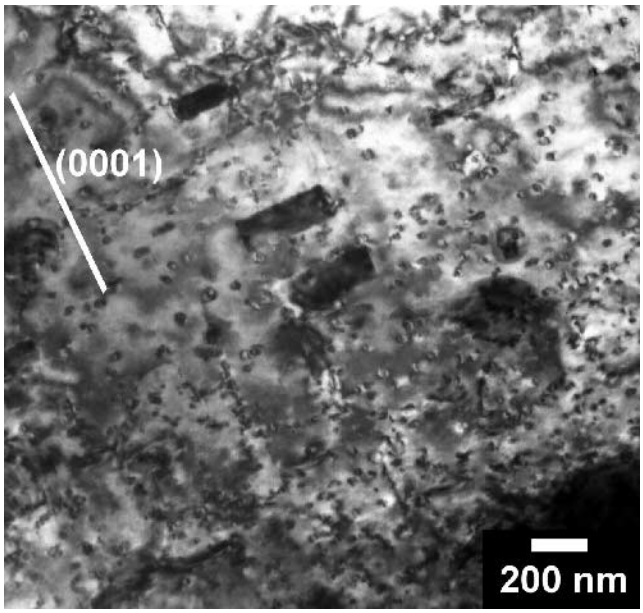

Fig. 5—Fine discs of Mn_2Sc phase parallel to basal planes of α-Mg matrix and coarse rods of $Mg_{12}Ce$ phase elongated in the $[0001]_{Mg}$ direction. Near $[1\bar{1}00]_{Mg}$ pole, bright field in $(0002)_{Mg}$ reflection.

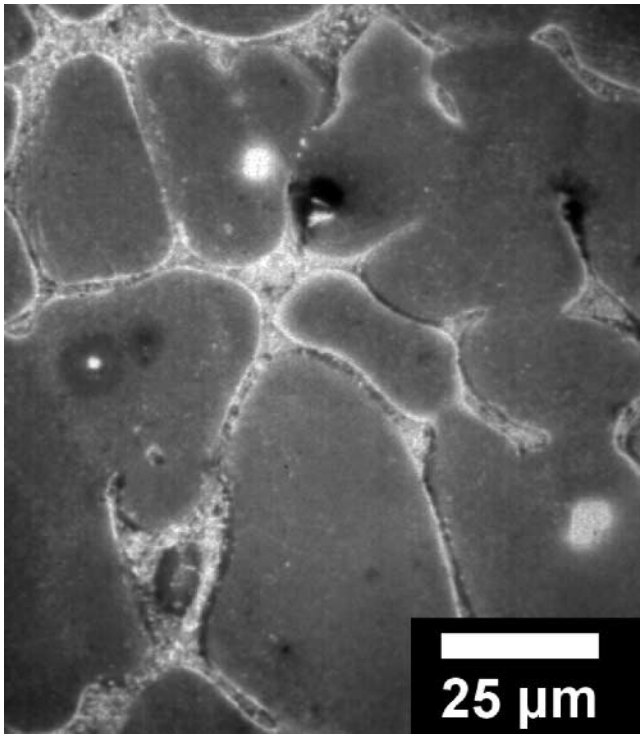

Fig. 6—Scanning electron microscopy of MgSc6Ce4Mn1 annealed at 325 °C/95 h.

A grain boundary eutectic of the Mg-Ce system (a-Mg matrix and $Mg_{12}Ce$ phase) persists during a T5 treatment and also during a long high-temperature exposure due to the low solubility of Ce (Figure 6).

The highly beneficial effect of the addition of Mn on the creep resistance of Mg-Sc alloys is evident (Figure 7). The

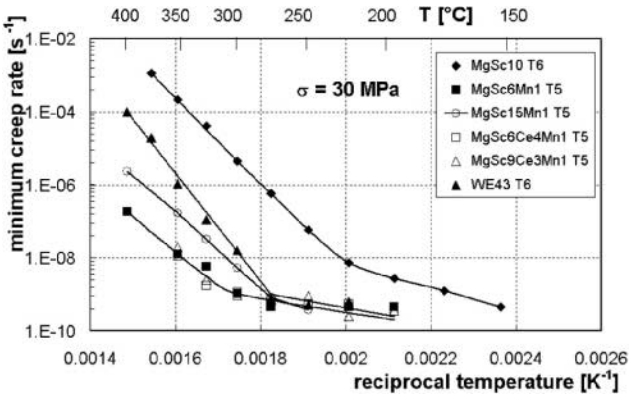

Fig. 7—Temperature dependence of minimum creep rate for MgSc(Ce)Mn alloys with high Sc content compared to binary Mg-Sc and WE43 alloys.

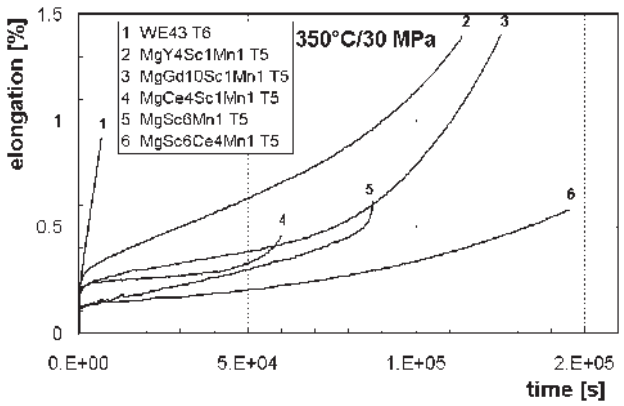

Fig. 8—Creep curves at 350 °C and 30 MPa.

ternary Mg-Sc-Mn and quaternary Mg-Sc-Ce-Mn alloys in the T5 state are superior to the WE43 alloy (T6) at temperatures over 275 °C and are comparable to HZ32A in the T5 state (the minimum creep rate at 300 °C and 30 MPa $\sim 1.10^{-9}$ s^{-1}— estimated value from Reference 13). At lower temperatures, the minimum creep rates in all alloys are close and comparable to those of WE43. No significant difference in creep rates of as-cast and T5-treated alloys was observed.

The transition temperature dividing the ranges with different activation energy extends to higher temperatures compared to the Mg-Sc alloys. The stress exponent n at 300 °C equals 5 for the ternary alloys and 3 for the quaternary alloys up to 40 MPa and increases to 10 at high stresses (Table II).

C. *Mg-Sc-RE-Mn Alloys with Low Sc Content*

As was the case for high Sc content alloys, only a T5 treatment was performed in order not to lose the advantage of producing a fine dispersion of Mn_2Sc. Figure 8 shows the creep curves for 350 °C and 30 MPa for various alloys with high and low Sc contents after a T5 treatment. All alloys contain approximately 1.5 wt pct Mn. The minimum creep rates achieved lie about one to two orders of magnitude lower than those for WE43 (T6) and are comparable to minimum creep rates of HZ32 (T5)—minimum creep rate at 300 °C and 44 MPa $\sim 9 \cdot 10^{-9}$ s^{-1} (estimated value from Reference 13). An excess of Sc does not improve the min-

imum creep rates significantly but does decrease the elongation in primary creep. The TEM of all Mg alloys with a low Sc content after creep exposure at 350 °C revealed a dense dispersion of basal discs of Mn_2Sc as the striking feature in the microstructure (Figure 9). A triangular arrangement of coarse prismatic plates of stable Mg_5Gd was observed in alloys containing Gd, but only in the vicinity of a dissolving grain boundary eutectic. The $Mg_{24}Y_5$ equilibrium phase was found only in the grain boundaries in the MgY4Sc1Mn1 alloy. Rare rectangular particles of the $Mg_{12}Ce$ stable phase were observed in the grain interior of the MgCe3Sc1Mn1 alloy. Complex precipitation processes take place during isochronal and isothermal annealing in the relevant temperature range for creep properties.[14,15] In addition to the precipitation of basal discs, Mn_2Sc, which is the main cause for the minima in changes in relative resistivity (Figure 10) of all low Sc content alloys, transient or equilibrium phases, characteristic for the Mg-RE and Mn-RE systems, also precipitate. The *c* base-centered orthorhombic phase (cbco, $a = 2.a_{Mg}$, $b = 8.d_{Mg}(1\bar{1}00)$, $c = c_{Mg}$, $[0001]_{cbco} \mid [0001]_{Mg}$, $<100>_{cbco} \mid <11\bar{2}0>_{Mg}$) precipitates in the form of plates parallel to all equivalent $\{11\bar{2}0\}$ prismatic planes of the α-Mg matrix in Y- and Gd-containing alloys. In MgGd10Sc1Mn1, this phase is responsible for the local minimum in relative resistivity at 280 °C. All morphological varieties of the $Mg_{12}Ce$ phase observed in the as-cast MgCe4Sc1Mn1 alloy transform into coarser rods of this phase on annealing up to the temperature of the main minimum. The hexagonal transient phase containing Mn and Y or Gd ($a = 2.d_{Mg}(1\bar{1}00)$, $c = c_{Mg}$, $[0001]_{hp} \mid [0001]_{Mg}$, $\{1\bar{1}00\}_{hp} \mid \{11\bar{2}0\}_{Mg}$) precipitates in the form of very thin basal plates in the MgY4Sc1Mn1 and MgGd5Sc1Mn1 alloys (Figure 11).

The same complex precipitation microstructure is responsible for the peak-age hardening, namely, simultaneous precipitation of all phases described previously (Mn_2Sc, cbco, hexagonal basal plates) in MgY4Sc1Mn1 and MgGd5Sc1Mn1 alloys, Mn_2Sc and cbco in MgGd10Sc1Mn1 (Figure 12), and $Mg_{12}Ce$ simultaneously with Mn_2Sc in MgCe4Sc1Mn1. These complex precipitation processes take place also during the creep tests of as-cast alloys at elevated and high temperatures. The temperature dependences of the minimum creep rates at 40 MPa of as-cast low Sc content alloys are compared with those of as-cast WE63 in Figure 13. All alloys are superior to WE63. The temperature dependence consists of two ranges with different activation energies for Gd-containing alloys. An anomalous low minimum creep rate was observed in MgY4Sc1Mn1 at 250 °C. The creep process is so irregular and the rates so low at these temperatures and stresses that it is difficult to define the minimum creep rate unambiguously.

The stress dependences of the minimum creep rates at 300 °C yielded a value of the stress exponent *n* close to 8 for Gd- and Y-containing alloys and 6 for the MgCe3Sc1Mn1 alloy (Table II).

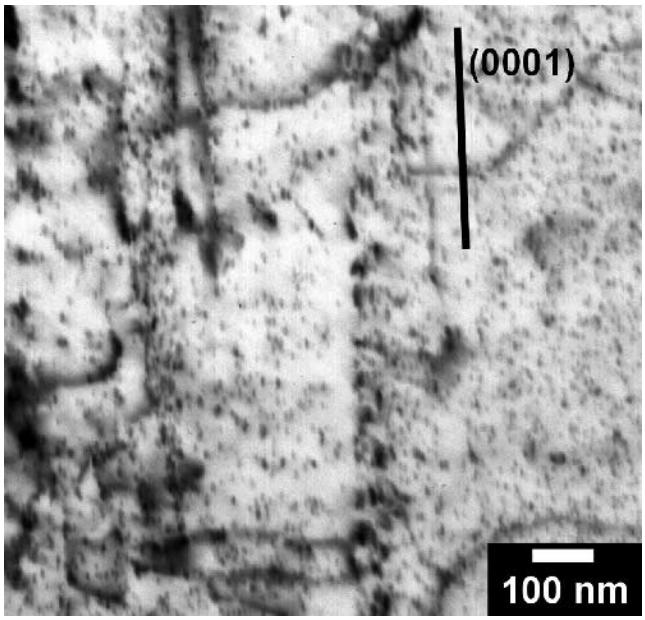

Fig. 9—Fine dispersion of Mn_2Sc phase basal discs in MgGd5Sc1Mn1 crept at 350 °C and 30 MPa. Bright field near $[11\bar{2}0]_{Mg}$ pole, $(\bar{1}10\bar{1})_{Mg}$ reflection.

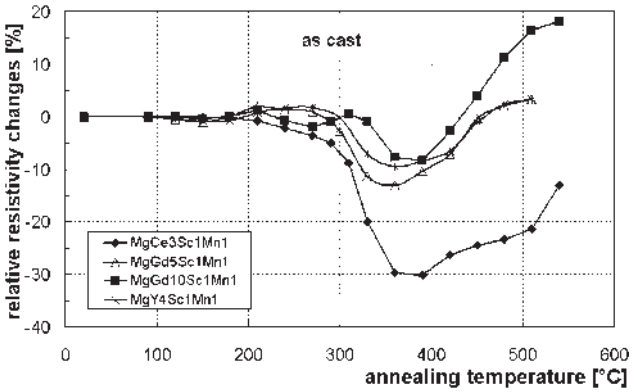

Fig. 10—Relative resistivity response measured at 77 K to isochronal annealing for Mg alloys with low Sc content.

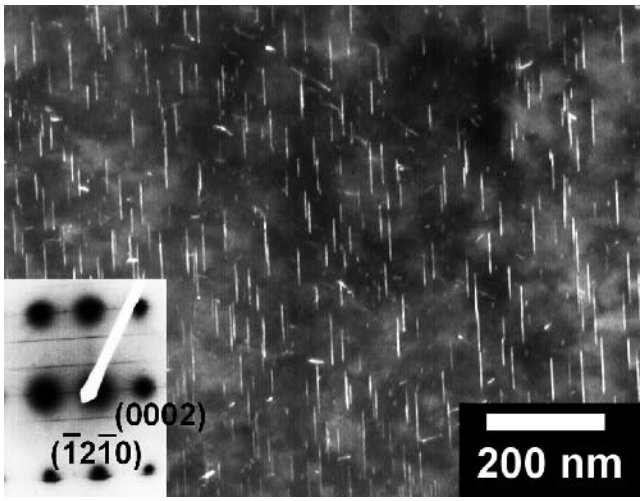

Fig. 11—Very thin basal plates of transient hexagonal phase containing Y and Mn in MgY4Sc1Mn1 isochronally annealed up to 360 °C. Dark field in $(10\bar{1}0)_{hp}$ reflection (streaks) of hexagonal plates, $[10\bar{1}0]_{Mg}$ pole, and $[1\bar{2}10]_{hp}$ pole (see inset).

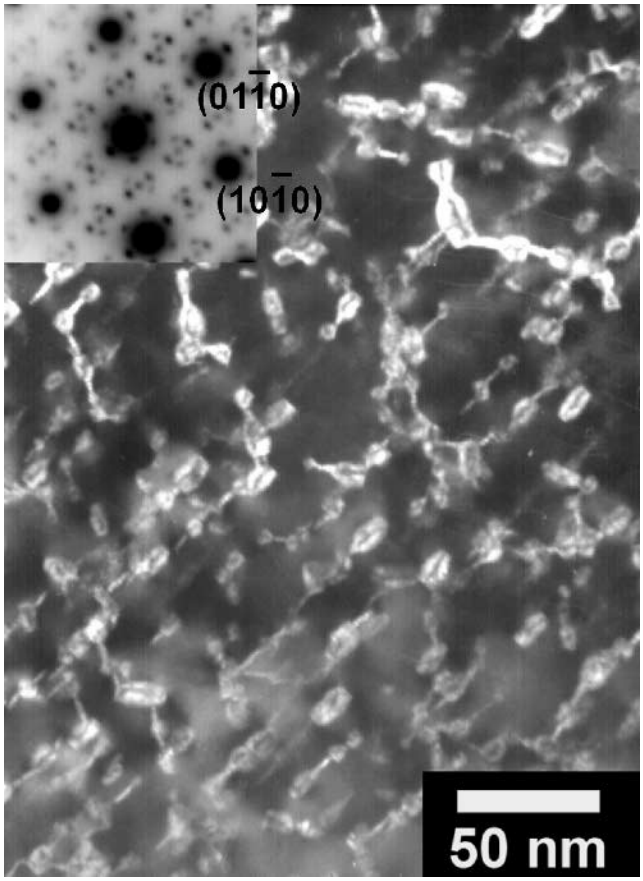

Fig. 12—MgGd10Sc1Mn1 after T5 temper, dark-field image of cbco phase, $[0001]_{Mg}$ pole (see inset).

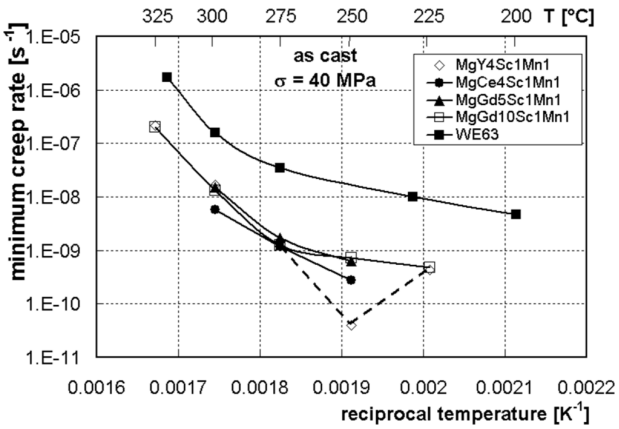

Fig. 13—Temperature dependence of minimum creep rate for Mg-RE-Sc-Mn alloys with low Sc content compared to WE63 alloy.

IV. DISCUSSION

The creep behavior of binary Mg-Sc alloys reflects the insignificant effect of the precipitation. Also, the Q_C values for alloys with different Sc contents after various treatments differ only slightly, *viz.* Q_C ~40 to 80 kJ/mol and ~210 to 260 kJ/mol for the low- and high-temperature range (Table III). There is no systematic dependence on either the Sc content or a heat treatment.[9] Improvement in the creep resistance with increasing Sc content should be attributed to the elastic interaction of dislocations with solute atoms.

Table III. Creep Activation Energies Q_C for Various Alloys at 40 MPa in the Temperature Range Denoted

Alloy	Temper	Temperature Range (°C)	Creep Activation Energy (kJ/mol)
MgSc10	T6	150 to 240	63
		240 to 375	224
MgSc11	T6	150 to 225	72
		225 to 325	262
MgSc15	T6	150 to 240	50
		240 to 375	216
MgSc19	T6	150 to 260	48
		260 to 375	233
MgSc6Mn1	T5	200 to 310	60
		310 to 400	161
MgSc15Mn1	T5	200 to 275	60
		275 to 400	197
MgSc6Ce4Mn1	T5	200 to 310	60
		310 to 400	161
MgSc9Ce3Mn1	T5	200 to 310	60
		310 to 400	161
MgGd10Sc1Mn1	as cast	225 to 275	58
		275 to 325	277
MgGd10Sc1Mn1	T5	225 to 275	65
MgGd5Sc1Mn1	as cast	250 to 275	58
		275 to 300	277
MgY4Sc1Mn1	as cast	250 to 325	351
MgY4Sc1Mn1	T5	250 to 325	392
MgCe3Sc1Mn1	as cast	250 to 300	152
MgCe3Sc1Mn1	T5	250 to 300	102

The high creep resistance of high Sc content alloys containing Mn at high temperatures must be ascribed to the effect of the dense distribution of fine particles of Mn_2Sc. This phase is very stable both thermally and morphologically up to at least 350 °C, as was observed after long creep exposure, with the same density and size as in the T5 temper. The effectiveness of spherically shaped particles (in MgSc15Mn1) is lower than that of disc-shaped particles parallel to the basal planes of the α-Mg matrix (in other alloys). This fact is consistent with the assumption that creep is controlled by the cross-slip of basal dislocations or nonbasal slip in the high-temperature range, as platelike particles in the basal planes are stronger obstacles to basal dislocations cross-slipping to the prismatic planes and to prismatic slip than spherical particles.[16,17] The values of the apparent activation energy determined for the high-temperature range were only slightly lower than those for Mg-Sc alloys (Q_C ~200 kJ/mol for MgSc15Mn1 and Q_C ~160 kJ/mol for other alloys (Table III)). Coarse rectangular precipitates of $Mg_{12}Ce$ in Ce-containing alloys have a low volume density and consequently only negligible effect on the creep rate. A stable grain boundary eutectic (Figure 7) can have some effect on the decrease of the minimum creep rate.

Alloys with significantly lower Sc content exhibit a very good creep resistance again, as the volume fraction of the

Mn_2Sc phase depends on the Mn content, which was practically the same as in alloys with a high Sc content. The values of the apparent activation energy for MgGdScMn alloys do not differ substantially from those for WE63 or WE43 alloys in both temperature ranges (~60 kJ/mol and ~280 kJ/mol (Table III)). This value in the high-temperature range is slightly higher for the MgYScMn alloy (Table III). Practically the same values of minimum creep rate and its temperature dependences were obtained both for the as-cast and the T5-treated alloys, including the anomaly mentioned in Figure 13. This is obvious for the Gd-containing alloys since the T5 treatment took place at 200 °C. In the case of the MgCe4Sc1Mn1 alloy, the minimum creep rates at 250 °C are slightly lower than at 225 °C. This indicates that the stress-enhanced precipitation leading to the same structure regardless of the previous treatment may take place at these temperatures, particularly in the MgY4Sc1Mn1 alloy.

The increase in the changes in relative resistivity compared to those for the initial value at high temperatures in isochronal annealing signifies dissolution of the equilibrium phase in the grain boundary eutectic in MgGdScMn and MgYScMn alloys with a low Sc content also during high-temperature creep (Figure 10). This leads to an increase in the RE concentration and eventually continuing precipitation and growth of precipitates in the matrix. This process affects the creep behavior and can influence also the minimum creep rate and its temperature dependence. A similar but weaker effect can occur in the Ce-containing alloy as the solubility of Ce in Mg is significantly lower than that of Gd and Y and the grain boundary eutectic is stable at least up to 570 °C. The values of the relative changes in resistivity do not even reach the initial zero level for that alloy.

An understanding of the relationship between microstructure and creep behavior in magnesium alloys with Sc, Mn, and RE should enable an objective, oriented design of a new creep-resistant alloy, which benefits from all the components of complex precipitation. The results of the creep tests and TEM observations of the MgY4Nd2Sc1Mn1 alloy confirmed that possibility (Figure 14). MgY4Nd2Sc1Mn1 after a T5 temper exhibits a superior creep resistance at 350 °C and 30 MPa over all other low Sc content alloys both in as-cast and T5 temper. The superiority over the WE-type alloys is clear at this temperature. The precipitation structure after a T5 temper (250 °C/40 h) consists of a dense layer of triangularly arranged cbco phase plates along the grain boundary eutectic with a sparse distribution of this phase on dislocations within the grain (Figure 15). The stable β phase (isomorphous with Mg_5Gd) precipitates during annealing at 250 °C in the same triangular arrangement of prismatic plates as in the WE and MgGd alloys simultaneously with the fine basal discs of Mn_2Sc and very thin hexagonal basal plates of a Mn- and RE-containing transient phase (Figure 16). A different precipitation structure in the as-cast and T5-treated alloy leads to a different structure at the start of a creep test at 350 °C and consequently to better creep properties of the T5-treated alloy.

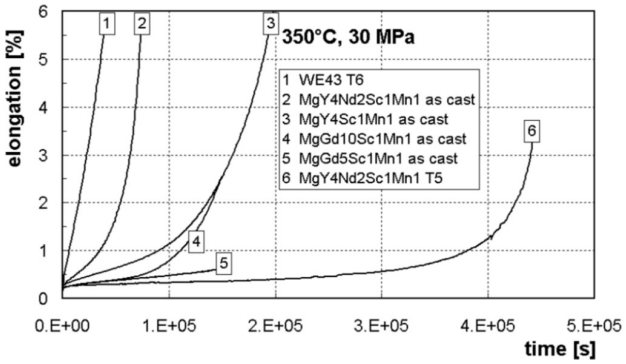

Fig. 14—Comparison of creep curves at 350 °C and 30 MPa.

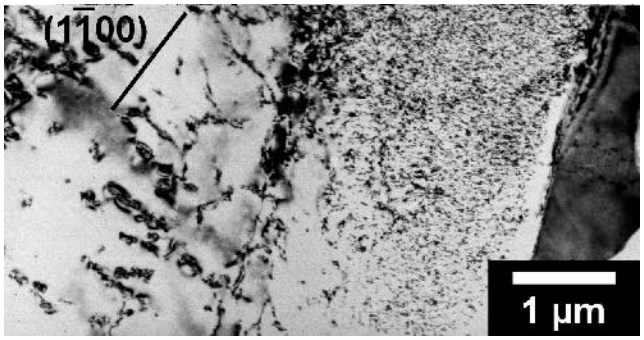

Fig. 15—Layer of dense arrangement of cbco phase plates along GB eutectic in T5-treated MgY4Nd2Sc1Mn1 alloy. Bright field near $[44\bar{8}3]_{Mg}$ pole, $(1\bar{1}00)_{Mg}$ reflection.

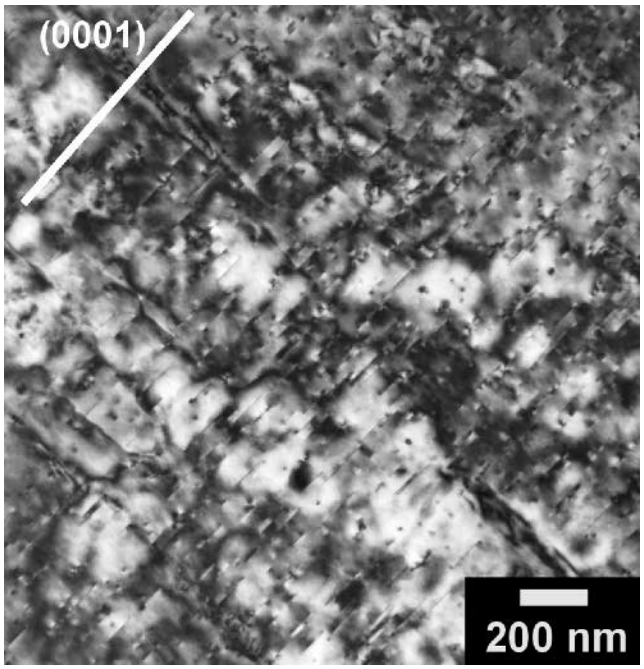

Fig. 16—Prismatic plates of stable β phase, thin basal plates of transient Mn, and Y-containing hexagonal phase and basal discs of Mn_2Sc phase in MgY4Nd2Sc1Mn1 annealed 45 h at 250 °C. Bright field in $(0002)_{Mg}$ reflection, $[52\bar{7}0]_{Mg}$ pole.

V. CONCLUSIONS

Binary Mg-Sc alloys exhibit negligible age hardening due to virtually no precipitation even at a high Sc content (19 wt pct), and also creep resistance of Mg-Sc alloys is inferior to that of WE alloys. The minimum creep rate decreases with increasing content of Sc. An elastic interaction of solutes with dislocations is the only significant effect of the Sc addition.

The addition of Mn (~1 wt pct) to Mg-Sc alloys improves the creep resistance substantially. Ternary Mg-Sc-Mn alloys are considerably superior to WE alloys especially at high temperatures. This is due to the dense dispersion of fine Mn_2Sc phase spherical particles, which are stable both in size and number, at least up to 350 °C. These particles have the form of fine discs parallel to the basal planes of the α-Mg matrix in MgScCeMn alloys. This form and orientation have a stronger effect on the cross-slip of basal dislocation or nonbasal slip and consequently on the creep resistance. The addition of Ce contributes to the improvement of creep resistance, most probably, due to the grain boundary eutectic and the precipitation of $Mg_{12}Ce$.

The beneficial effect of the basal discs of Mn_2Sc on the creep resistance at high temperatures is preserved in the MgREScMn alloys with a considerably lower Sc content (~1 wt pct). Quaternary alloys with a low Sc content are superior in creep to WE alloys at high temperatures. Prismatic plates of the cbco phase in a triangular arrangement and also the thin hexagonal basal plates containing Mn and RE contribute to the superiority in creep resistance at elevated temperatures.

An even more pronounced effect of the complex precipitation structure on the creep resistance of the modified WE alloy with Sc and Mn (~1 wt pct) demonstrated the possibility and efficacy of tailored design of complex high-performance Mg alloys.

ACKNOWLEDGMENTS

The support by the German Research Foundation (DFG), by the Czech Grant Agency (GACR Project No. 106/03/0903), and by the Ministry of Education of the Czech Republic within the framework of the research program MSM 113200002 is gratefully acknowledged.

REFERENCES

1. G.W. Lorimer: *Proc. London Conf. on Magnesium Technology*, H. Baker, ed., Institute of Metals, London, 1986, pp. 47-53.
2. I.J. Polmear: *Mater. Sci. Technol*., 1994, vol. 10, pp. 1-16.
3. T.B. Massalski: *Binary Alloy Phase Diagrams*, 2nd ed., ASM, Materials Park, OH, 1990, vol. 4, pp. 2545-6.
4. P. Vostrý, I. Stulíková, B. Smola, F. von Buch, and B.L. Mordike: in *Magnesium Alloys and Their Applications*, B.L. Mordike and K.U. Kainer, eds., Werkstoff-Informationsgeselschaft, Frankfurt, 1998, pp. 333-38.
5. B.L. Mordike and F. von Buch: *Magnesium Alloys and Their Applications*, K.U. Kainer, ed., Wiley-VCH Verlag, Weinheim, 2000, pp. 35-40.
6. B.L. Mordike: *Mater. Sci. Eng. A*, 2002, vol. 324, pp. 103-12.
7. B.L. Mordike and I. Stulíková: *Proc. Int. Conf. Metallic Light Alloys*, Institution of Metallurgists, London, 1983, pp. 146-53.
8. W. Henning and B.L. Mordike: *Proc. ICSMA 7*, Montreal, 1985, pp. 803-08.
9. F. von Buch: Ph.D. Thesis, TU-Clausthal, Clausthal-Zellerfeld, 1999.
10. F. von Buch, J. Lietzau, B.L. Mordike, A. Pisch, and R. Schmid-Fetzer: *Mater. Sci. Eng. A*, 1999, vol. 263, pp. 1-7.
11. B. Smola, I. Stulíková, J. Pelcová, F. von Buch, and B.L. Mordike: *Phys. Status. Solidi. (A)*, 2002, vol. 191, pp. 305-16.
12. I. Stulíková, B. Smola, J. Pelcová, F. von Buch, and B.L. Mordike: *Magnesium 2000*, A. Aghion and E. Eliezer, eds., MRI, Beer Sheva, 2000, pp. 218-25.
13. Magnesium Elektron Ltd., Manchester, United Kingdom, 1993.
14. I. Stulíková, B. Smola, F. von Buch, and B.L. Mordike: *Mat.-Wiss. Werkstofftech*., 2001, vol. 32, pp. 20-24.
15. B. Smola, I. Stulíková, J. Pelcová, F. von Buch, and B.L. Mordike: *Z. Metallkd*., 2003, vol. 94, pp. 553-58.
16. J.F. Nie: *Scripta Mater*., 2003, vol. 48, pp. 1009-15.
17. B. Smola, I. Stulíková, F. von Buch, and B.L. Mordike: *Mater. Sci. Eng. A*, 2002, vol. 324, pp. 113-17.